APPENDIX D. PRELIMINARY DEPLOYMENT AND EVALUATION OF GEOPHONE SENSORS FOR MONITORING WAVE ACTIVITY: *GEOMOTESHIELD*

Note that this appendix contains the Honors Thesis published by Eve Latrhop at Oregon State University with Drs. Michael Olsen, Ben Leshchinsky, and Andrew Senogles as committee members. Minor updates have been made.

1.1 ABSTRACT

This study focuses specifically on the investigation of a new, inexpensive geophone system and its application to monitor wave activity. Studies of seismic observations of coastal cliffs suggest that ground motions generated from local ocean waves may provide a surrogate to limited wave buoy data to quantify the wave contact and impact on the coastal cliff. Ground motion monitoring of ocean waves also has the potential to improve our understanding of coastal processes by understanding not only how frequently waves impact the coastal cliff but also the accelerations (shaking) present in the cliff as a result of the impact. A preliminary test was conducted using the GeoMoteShield geophone system at varying gain settings (4, 8 and 16 x gain levels) with three sensors located at different distances from the bluff face. The results imply that the degree of ground motion detected is dependent on a variety of parameters: distance from the bluff, the magnitude of wave energy etc. When tidal and significant wave height levels measured from a nearby buoy were larger, a stronger correlation was observed between the amplitude recorded at the sensors compared with the significant wave height. There is also a correlation between the system's ability to predict wave action and the sensors proximity to the cliff top edge. Sensors placed too far from the cliff's edge were affected too much by ambient traffic sounds.

Key Words: Geophone, Coastal Erosion, Cliff Erosion, Coastal Monitoring

1.2 INTRODUCTION/OVERVIEW

Rising sea levels and extreme coastal weather events pose significant risks for the safety, reliability and effectiveness of infrastructure and operations along the coast. In the State of Oregon alone, coastal erosion and landslides account for millions of dollars in damage to Oregon Department of Transportation's (ODOT) coastal infrastructure each year. During a five-year period from 1995-2000, approximately $22.3 million was spent on landslide repairs along U.S. Highway 101, a vital lifeline highway that runs along the west coast of Washington, Oregon, and California [Hormann, 2012]. The average rate of long-term shoreline change for the entire Pacific North Coast is growing at a rate 0.9 meter per year (m/yr) (+/- 0.07 m/yr.) [*Ruggiero, P.,* 2013]. In particular, the Tillamook County area of Oregon is identified as a location with the most significant erosion observed. A quarter of the town's population lives within a half mile Pacific Ocean and 40 percent of the coastline there is eroding at rates of more than 0.9m a year [*Mills, A.,* 2018]

Wave action in the PNW is recognized for its severity and is one of the major contributors to coastal erosion. Winter storms commonly generate deepwater significant wave heights (SWH) greater than 10 m (about one event of this magnitude per year). The largest storms in the region have generated SWHs in the range of 14 to 15 m [*Allan and Komar*, 2002]. Tall, long-period waves (averaging about 3 m in height and 12 to 13 s in period), high-water levels, and a west-southwest direction of wave approach characterize the winter months (November through February), whereas smaller waves (1-m SWHs and 8-s periods), low water levels, and wind and waves from the west-northwest are the typical summer (May through August) conditions [*Ruggiero, P.,* 2013].

Coastal bluff erosion occurs worldwide, not just in Oregon. Despite being readily observable given the rapid pace of erosion, the processes are extremely difficult to measure. Landslides and coastal bluff erosion are common processes in this unstable environment, but the rates of movement are not well characterized. Recent studies on coastal cliffs [*Young and Guza,* 2011, *Dickerson and Pentney*, 2012, *Adams et al*., 2002 and *Earlie et al.*, 2015] suggest that ground motions generated by local ocean waves may provide a proxy to quantify the wave impacts on the cliffs, which has the potential to improve our overall understanding of coastal processes. These cliff seismic observations are gathered using a wide variety of systems and the accuracy of these systems are typically inversely proportional to the cost associated with developing them.

The overarching goal of this coastal monitoring project is to develop a more comprehensive data-driven framework for prioritizing coastal asset management for Oregon DOT. This honors thesis focuses specifically on the investigation of a new, inexpensive geophone system to be used in monitoring wave activity. The first objective is to determine how to effectively use the *GeoMoteShield* geophone systems and produce a basic framework for on the system with clear step by step instructions. The second objective is to perform a preliminary investigation of the suitability of this system to monitor on-site wave activity, including evaluation of optimal gain settings and sensor placement.

1.2.1 Scope of Document

This document provides detailed, specific, and standard operating procedures for data acquisition, storage, and processing associated with using the *GeoMoteShield* wireless geophone system, which was produced by Marc Rubin, CEO of Geomote Systems, Inc. Part I covers the specifics and standard operating procedures of the *GeoMoteShield* geophone systems (Objective #1). It also includes instructions on how to extract the data and a basic procedure for analyzing the data. Part 2 focuses specifically on a preliminary test (Objective #2) conducted using the system and an analysis of the results to determine the viability of the system in long term coastal monitoring.

1.3 BACKGROUND INFORMATION

Prior to discussing the components of the systems and the preliminary analysis of data collected, a brief background on seismic instrumentation and the use of seismic data to monitor wave activity along coastal cliffs is provided.

1.3.1 Wave recording

A geophone system detects ground movements (i.e., velocities) produced by waves and transforms those motions into electric pulses to capture the seismic response at a location. The strongest seismic waves are generated by earthquakes due to a sudden breaking or expansion of rock within the earth. However, seismic waves can also be generated through falling weights (e.g., hammers) or ambient sources such as ocean waves (*Seismic Waves,* 2020*)*. The geophone system is detecting a variety of seismic waves (body and surface waves) that are produced by the ocean waves as they break against the cliff face. As the waves break along the cliff face, they generate seismic waves that travel through the median of the cliff. The seismic waves that are of

particular interested are the body waves. The body waves impact the cliff and causes the cliff particles to shift.

Seismic body waves are fundamentally composed of two type of waves: compressional or longitudinal waves and shear or transverse waves, also known as P (primary) waves and S (secondary) waves, respectively (*Seismic Waves,* 2020*)*.

P-waves (compression waves) are the fastest seismic waves and are the first to arrive at a location away from the seismic source. P-waves travel longitudinally in the propagation direction. In earthquakes, these waves typically do not cause much earthquake damage. P-waves can be transmitted through gases, solids and fluids (*Seismic Waves,* 2020*)*.

S-waves (shear waves) travel slower than P-waves. S-waves travel in an alternative transverse motion perpendicular to the direction of propagation. S-waves only travel and propagate through solid mediums and can cause significant damage in seismic based events. They do not travel through fluids (*Seismic Waves,* 2020*)*.

1.3.2 History of Seismic Data along Cliffs

Utilization of geophones to obtain detailed observations of cliff top ground motions generated by local ocean waves has been relatively limited. Nevertheless, recent studies of seismic observations of coastal cliffs suggests that ground motion generated from local ocean waves may provide a surrogate to quantify wave impacts [*Young and Guza*, 2013], which can be difficult to accurately quantify using other techniques. Ground motion monitoring of ocean waves also has the potential to improve our understanding of coastal processes by enabling quantification of wave activity as well as ground accelerations generated by wave activity. Cliff ground motion can be elevated above natural background levels dues to wave action and categorized into two general frequency bands, higher and low-frequency cliff motion [*Young and Guza*, 2013]. Ocean waves that directly impact the cliff [*Adams et al.,* 2002] or the front shore platform [*Dickerson and Pentney,* 2012] are classified as higher frequency cliff motion or "shaking" with a frequency >0.3 Hz. Individual swells or single frequency waves [*Adams et al*., 2005] and infragravity waves [*Young et al*., 2011, 2012] are classified as low-frequency cliff motion with a frequency of $0.01 < 0.1$ Hz. Observations show that these cliff ground motion responses varied and are influenced by a combination of tide level, incident wave energy, site morphology, ground composition and signal decay [*Young and Guza*, 2013]. Cliff shaking and flexing generally increase with greater incident wave height and water levels.

[*Young et. Al.*, *Dickerson and Pentney*, *Bossolasco et al.*, *Adams et al*., *Lim et. al., Earlie et al.*] have utilized seismometers to document significant ground motion (greater than the natural background levels) generated by local ocean waves. These studies focused on frequencies changing from 0.01 to 100Hz and had observational periods ranging from a week to a few months. Because there is yet not a consensus on what influences or controls the coastal seismic response caused by local waves, there is a not one specific system suggested and used in monitoring ground motion. A variety of systems have been utilized in previous research.

Bossolasco et al. [1973] compared observations on sites that analyzed real time microseisms records on top of cliffs. Site one was a few km inland on top of an ocean-front cliff (Genoa) and

another station was placed just on the shoreline (Vesima-Arenzano). Two primary methods were used with an aim to deduce their fundamental periods and evolutions of the cliffs. The first method consisted of the autocorrelation of microseisms as a random signal is derived. The second method consisted of frequently filtering the data, which is a more extensively used methods. The inland sites produced weaker single frequency motions, whereas the shore-line site produced approximately equal spectral densities/energy level for single and double frequency motions. It was concluded that the variation in breaking zones for the two stations caused the frequency of motion to be weaker at the inland site.

Adams et al. [2002] studied ground motion on top of a 10m high cliff located in central California where a bedrock platform was situated directly below the site. This site is characterized by 5-30m high sea cliffs and is decorated with irregularly spaced pocket beaches. The shore wave energies were derived from measurements recorded using a broadband seismometer that measured the ground velocity associated with cliff shanking while a RefTek L4C3D 1 Hz velocity transducers was attached to the system. The sensor recorded ground velocity in the vertical, north-south, and east-west direction at a sampling frequency of 50Hz. The velocity data recorded was analyzed through constructing a sum for each hour to yield a cumulative hourly shaking for each direction. This simplification reduced the data from 540,000 to 3 points per hour, the same intervals over which the wave and tidal data was reported. It showed that high frequency (1-25 Hz) waves induced cliff shaking which is depended on offshore wave conditions, shelf bathymetry and tide level. High frequency shaking from wave impacts is also dependent on the downward and seaward cliff flexing as incoming waves crests approach the cliff face [*Adams et al.*, 2005]. Observations show that at the cliff flexing decreased with increasing distance landward from the cliff edge.

Lim et. al. [2011] studied ground motions generated by ocean waves along a 180-m section of cliffs on the North Yorkshire coast in the United Kingdom. The cliffs are more than 70m in height and composed of mudstones, shale, siltstone, ironstone, and sandstone, and they are capped with a 15-m drape of glacial till [*Lim et al.,* 2010]. To further understand the relationship between coastal landforms and the range of processes that control their evolution, comparisons were made between the two actions through recording micro-seismic ground movements. A 4.5-Hz. Integrated seismic system tri-axial geophone was installed at the cliff top to measure wave-induced shaking of the cliff. The geophone system was mounted to a 1000-kg concrete block to dampen resonance. It was connected to a stand-alone quake seismometer (SAQS) data logger with a 24-bit digital convertor. Since resonance effects were found to influence the length of the seismic signal, data was gathered to determine the background seismic signals of the region. The background signals were filtered out and low frequency triggers caused by breaking waves were identified. A terrestrial lidar survey of the coastal corridor was used to quantify the foreshore morphology. These observations showed that critical tide levels occur when the wind directions coincide with the greatest fetch. Foreshore micro-topography is shown to have a significant influence on wave energy flux and impact timing at the cliff face.

Dickson and Pentney [2012] studied ground motions from ocean waves along a cross-shore transect cliff where seismometers were positioned at the cliff top recording in the 1-100Hz range. The sites were 50m and 200m inland and at the base of a 37m cliff in New Zealand. Four Geospace Technologies Mini Seis-Monitor 2 Hz sensors and broadband seismic recorders (Reftek 130-01/03) were deployed on a transect parallel to the wave pressure sensors where it

measured three directions of ground motion (vertical, north–south and east–west). The data was analyzed using a standard zero-down crossing technique to calculate wave statistics. Seismic data were divided into hourly files and time-synchronized using a GPS sensor attached to each instrument. Similar to other studies, they observed that ground motion was tidally modulated and would increase with increasing incident wave height and decreased with distance inland. Contrary to what *Adams et al*. [2002, 2005] observed, *Dickson and Pentney* [2010, 2012] found that during large wave events, cliff top ground motion was lowest at high tide and greatest at mid-low tide, therefore suggesting that cliff top motion is dependent on how wave energy dissipates on the seaward side of the elevated shore platform. Observations in North Yorkshire [*Lim and Rosser et. al.,* 2011] also suggests that topography influences ground motion supporting this observation.

Young et al. [2011] compared ground motions of the frequencies of ocean infragravity and swell waves (0.01 – 0.1 Hz) on top a coastal cliff in Southern California through monitoring inland ground motions and cliff base water fluctuation levels. The ground motion was measured at 100Hz with three Nano-metrics Compact Trillium broadband velocity seismometers at cross-shore. The system was located on top of the cliff at 0, 5, 10, 20, 40, 80, and 160 meters from the cliff top edge. Each positioned was measured for 2-4 weeks (November 2010 to April 2011). At high tide, the cliff top motions were found to be coherent and in phases with water levels of fluctuation at the cliff base, while the spectral levels were greater on the cliff top than they were inland. At low tide (ocean waves never met cliff base), the spectral levels on the cliff top were similar to the inland levels. In a follow-on study at the same location, *Young et al.* [2012] also observed ground motion along a cross-shore transect and determined that vertical ground motions (infragravity and single frequency levels) decreased rapidly inland with distance from the cliff edge. Between high and low tide, the frequency levels would decrease several orders of magnitude.

Young et al. [2013] compared ground motions between 8 sites with varying morphologies (rock slope, cliff, and sand beaches) that were located within 100m of the water line. For every site, a Nano-metrics Compact Trillium broadband velocity seismometer collected ground motion at 100Hz for at least 13 days and were buried approximately 90cm from the ground surface. Seismic data were divided into 1 hour segments, detrended, and processed with Fourier spectral methods. For all sites, local ocean waves generated ground motions between 0.01-40Hz in the cliff. Overall, the spectral shapes generated were consist across the shoreline sites, but site specific responses varied and were influenced by a combinations of factors: tide level, incident wave energy, site morphology, ground composition and signal decay, therefore backing the hypothesis that seismic observations are not a simple proxy for the wave-cliff interactions.

Lastly, *Earlie et al.* [2015] observed clifftop ground motions produced by storm waves along a 300 m stretch of uninhabited cliffed coastline southeast of Porthleven, UK. The cliff-top ground motion was recorded using a Nanometrics Compact Trillium broadband seismometer sampling at 100 Hz. Video was captured facing towards the cliff to provide a qualitative, but a detailed account of the hydrodynamics during the seismometer deployment. Terrestrial lidar surveys over a 2 week period showed a cliff face volume loss of 2 orders of magnitude larger than the long-term erosion rate. The results imply that erosion of coastal cliffs exposed to extreme storm waves is highly episodic. The long-term rates of cliff erosion will depend on the frequency and severity of extreme storm wave impacts the cliff is exposed to.

1.4 PART 1: SENSOR OPERATION

1.4.1 Hardware

The *GeoMoteShield* wireless geophone systems were originally produced by Rubin [2014], which focused on the efficiency of automatic wireless geohazard monitoring systems. The unit is designed to collect data continuously for days, weeks, or even months at a time at a high frequency (100 Hz). The geophone system contains several components integrated in a weather resistant control box (Figure 1): Three geophones (and wiring) to capture the signals (Figure 4), a digitization module to encode the signals, a computing platform to log and provide access to the data, and hardware to power the system. These components are integrated in a control box (14.5in. x 10.5in. x 5in.), which contains two cable glands: one for the three geophone cables and one for the power cables to connect to the power source.

The digitization module (black case in Figure 2) is designed on an Arduino Fio wireless mote platform (digitizer). The system contains a three high precision-low noise analog-to-digital converter (ADC) that provides 24-bit precision and collects data at 100 Hz. The Arduino Fio wireless mote platform connects to an external Raspberry Pi system through a USB connection. An external hard drive is attached to the Pi system to contain the operating systems as well as log the data. The system is also equipped with two, hot swappable USB flash drives to provide redundant backups of the data after each collection set (Figure 3).

The system is also equipped with a battery-powered Real time clock (RTC) to keep track of time when the Pi system is off (Set to Pacific Standard Time). Power to the Raspberry Pi system is supplied through a micro-USB that connects the system to a solar panel charge controller and battery regulator via a CPT 15C DC/DC converter as shown in Figure 1. A 12 V battery was used as the power source; however, a solar panel can be installed to provide continuous power to the system.

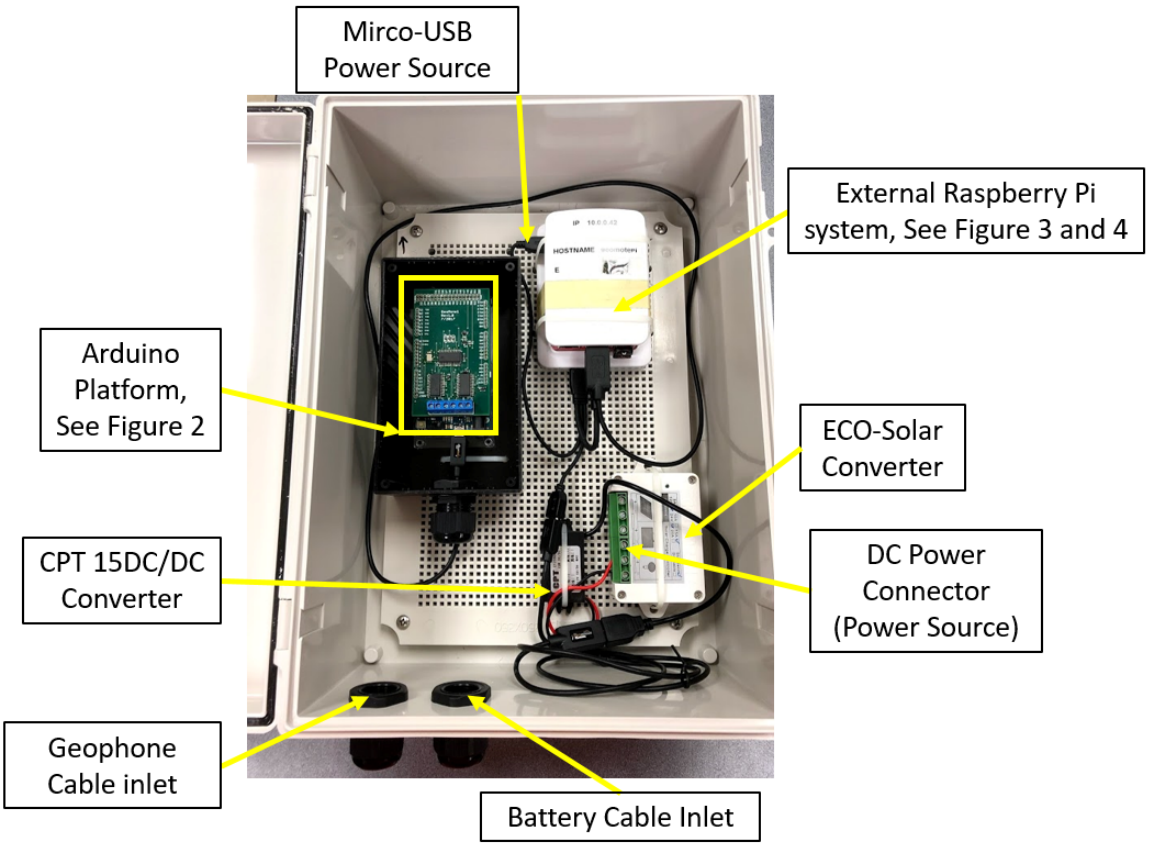

Figure 1. Picture of components inside *GeoMoteShield* Geophone system box designed by Marc Rubin.

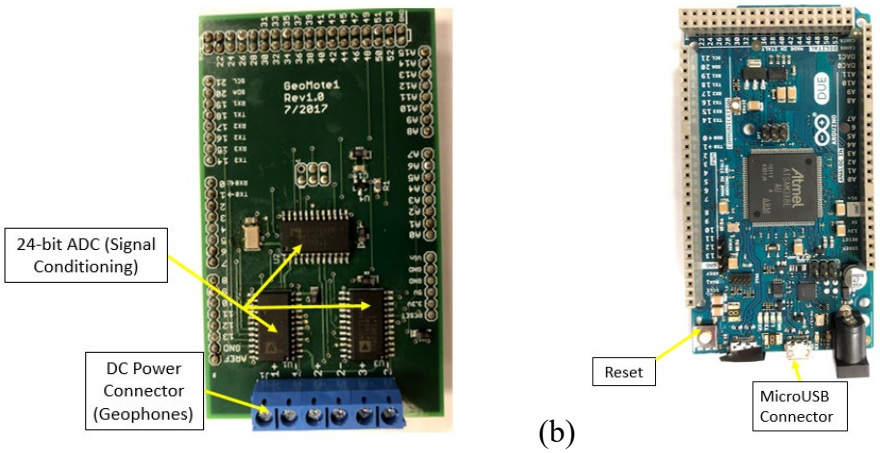

Figure 2. Detail of Arduino Fio wireless mote platform inside *GeoMoteShield* system, (a) - layer1 and (b) - layer 2.

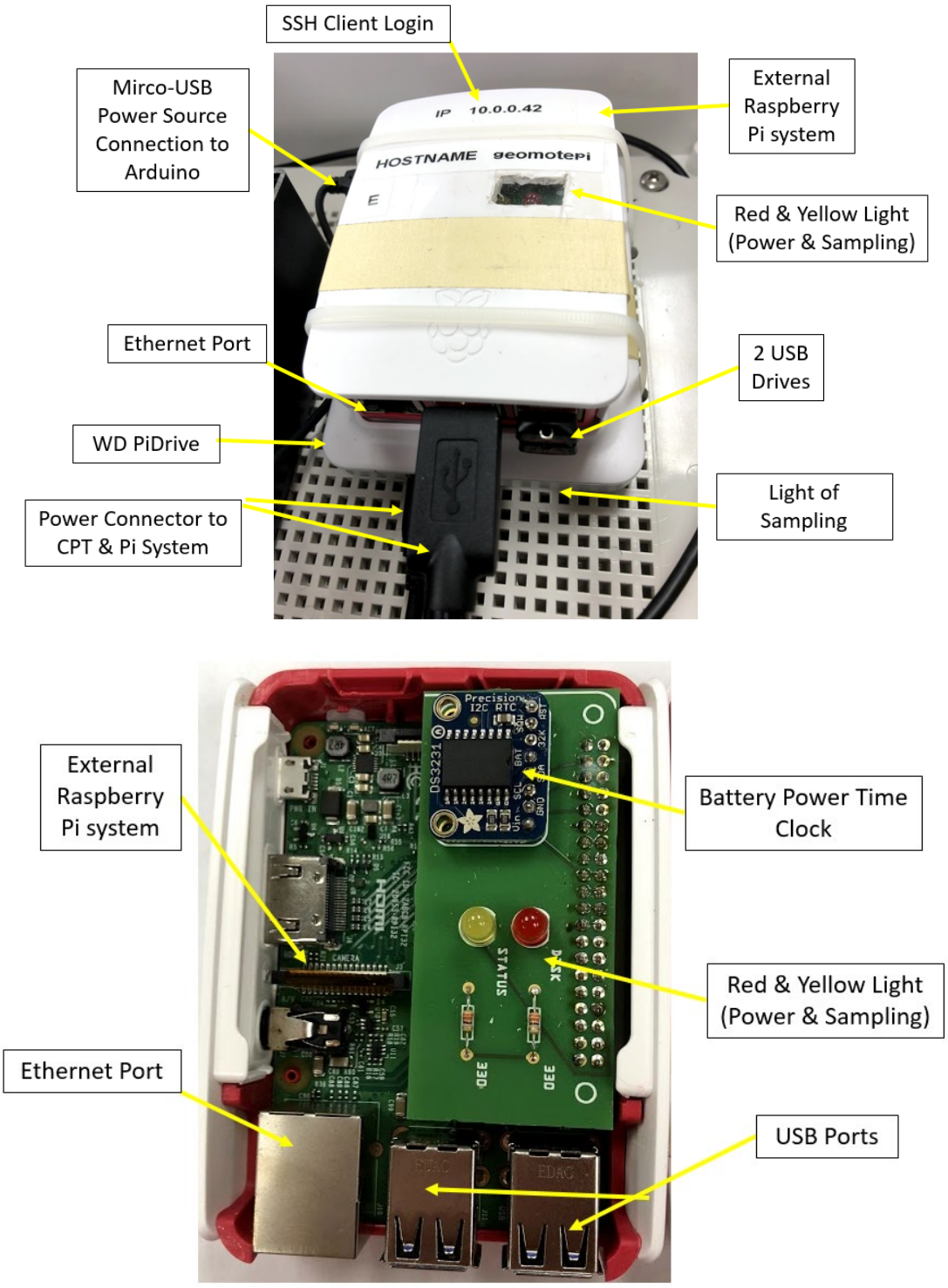

Figure 3. Detail of Raspberry Pi system inside the GeoMoteShield system.

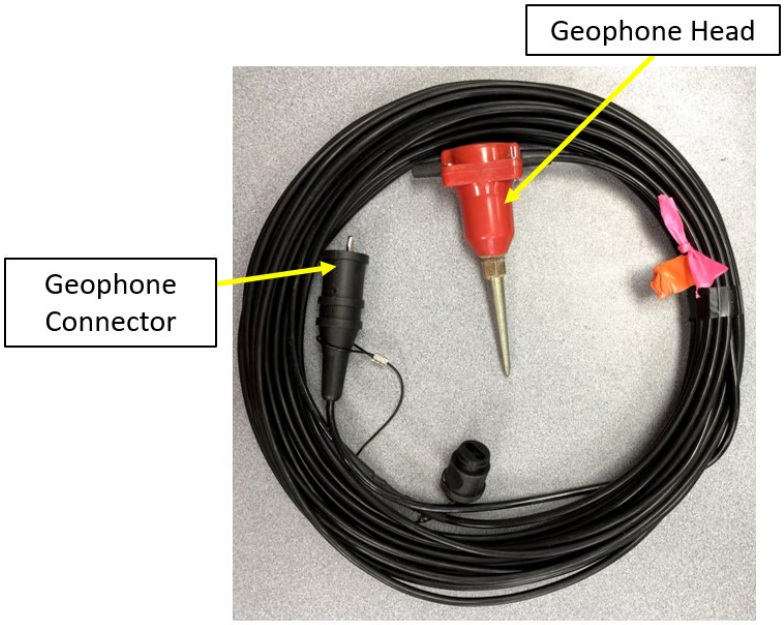

Figure 4. Detail of Geophone sensors and cable.

1.4.2 Installation Procedure

Instrument installation occurs in four primary stages: 1) construction of the geophone system, 2) use of the website app to configure and test the unit, 3) installation of the geophone systems in the field, and 4) accessing Raspberry Pi system to capture data via a wireless connection on site. Note that these instructions are for a temporary deployment. A more permanent installation would require a more rigorous setup.

1.4.2.1 Lab Configuration of the Geophone system

- The first step towards constructing the geophone unit consists of connecting the three-geophone sensors to the analog to digital converter system (Figure 2). Once that is complete, insert the USB flash drives formatted as FAT volumes to the Raspberry Pi system. Connect the digitizer and CPT converter to the Pi system.

- Power the Pi system in one of two ways (Battery, 12V or Solar, 24V). Connect the power source to the respective positive and negative terminals. The unit will boot up and start collecting time stamped (timed) seismic data. The unit is sampling when the Yellow LED on the face of the Pi system is on.

- *Note:* The USB flash drives are interchangeable. Only unplug USB drives if the red light is off on the front of the Pi system. Only unplug one of the USB drives at a time to pull data. It is safer to access the Pi system Secure Shell (SSH) to shut off the system first.

1.4.2.2 Accessing the control interface to configure and test the unit

- To access the control interface associated with geophone system, manually set your computer's ethernet IP address to: **10.0.0.1**. Connect your computer with the Pi system through the ethernet cable connection. Access the interface with a web browser at: http://10.0.0.42:500. One may need to submit the address multiples times to connect.

- *Note:* If the site does not connect, make sure the Raspberry Pi is operational (check the yellow light to ensure it is collecting data). If the yellow led is not on, check to make sure the ethernet cord is securely connected to the Computer and Raspberry Pi system.

- Once you have accessed the web app, there are four separate pages: *Home, Configure, View Data, View logs* and *Download.*

    - The *Home subpage* provides a live display of the geophone recordings shown on 3 separate graphs (one for each channel) and the digitizer's status (Figure 5).

    - The *Configure* page sets the geophone sensors to collect data at varying gain levels: 4, 8, 16, 32, 64, and 128. As the gain setting increases, the sensitivity of the system increases, enabling softer sounds\motions to be captured at the expense of softer sounds\motions being cut off; however, when the gain level decreases, louder sounds\motions will be captured while softer sounds\motions will not be detected (Figure 6).

    - The *View Data subpage* displays all datasets that have been collected by the unit and displays a table recording the seismic data (Figure 7).

    - The *View Logs subpage* displays a log of the digitizer's log during a specific collection time (Figure 8).

    - The *Download subpage* can be used to extract the data from the Raspberry Pi system which requires an ftp program such as ***FileZilla*** (Figure 9).

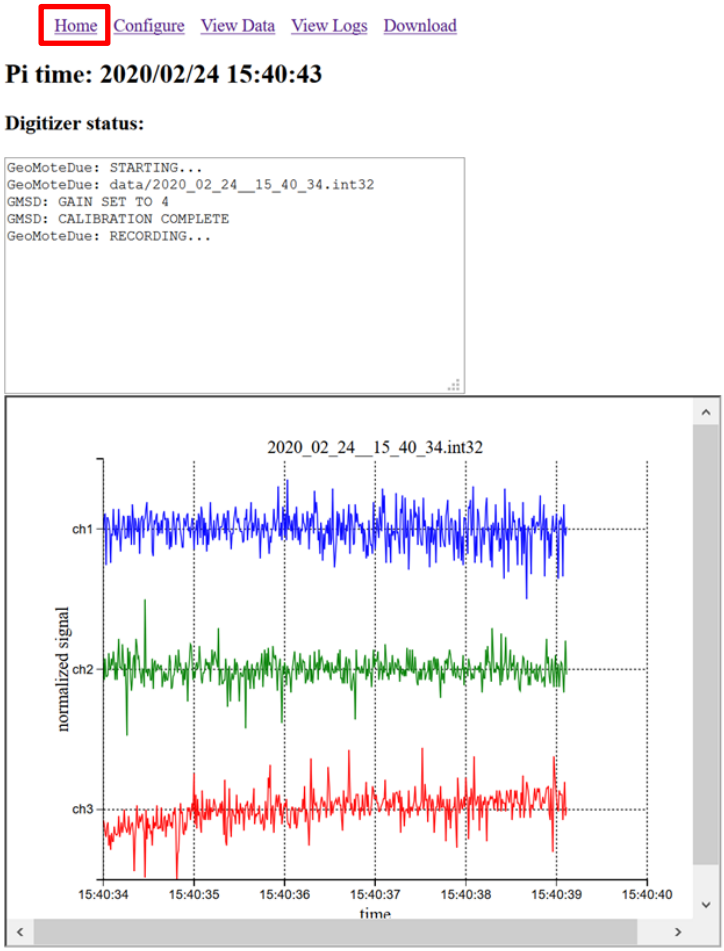

Figure 5. Home subpage showing a preview of the data collected.

Figure 6. Configure subpage where the user can set the desired gain level.

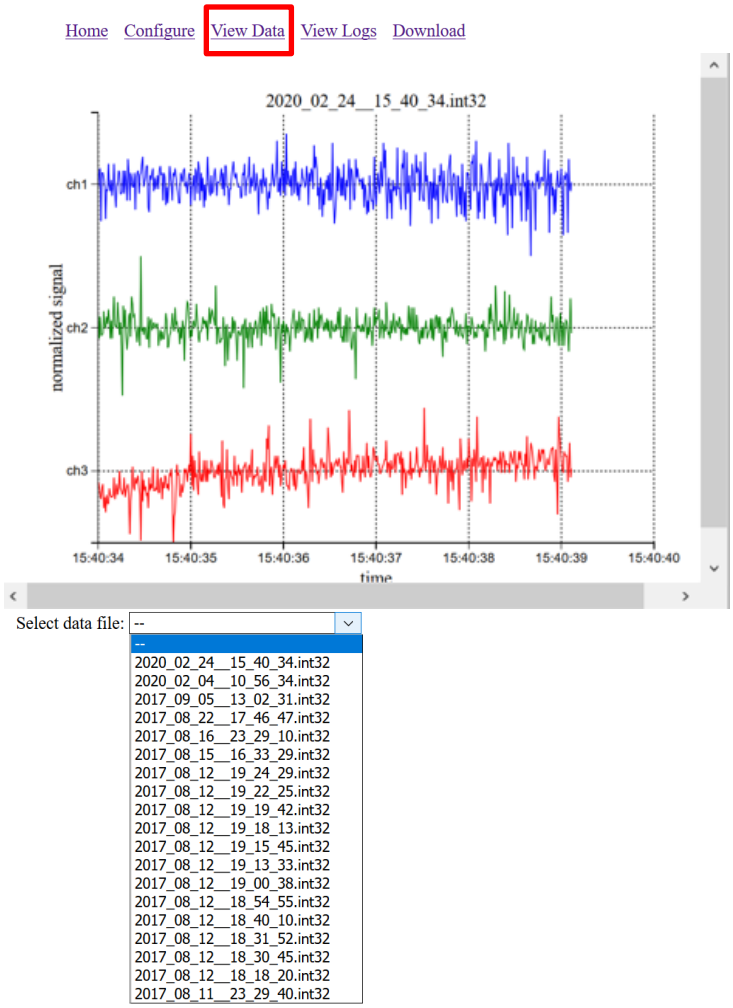

Figure 7. View data subpage where the user can explore datasets collected on the sensor.

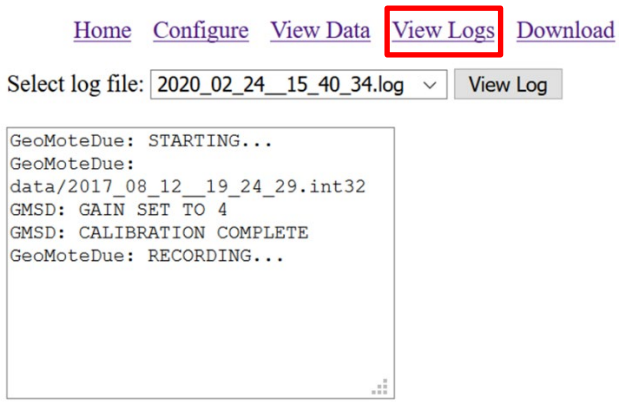

Figure 8. View log subpage where errors are reported.

Figure 9. Download subpage, which simply refers the user to FileZilla.

1.4.2.3 Installation of the geophone unit in the field (Applicable to Preliminary Test in Part 2) for a temporary deployment.

- Once in the field, the first step is to determine optimal locations to place the geophone sensors, the control unit, and power source. The process of determining the ideal locations to install the sensors is dependent on the intended usage purpose. Things to consider in placement of the sensors include proximity to the sources to monitor (e.g., ocean waves), locations of sources of noise, and locations where they can be hidden from the public eye or from animal disturbance to avoid tampering.

- Configure the geophone unit prior to installing the system into the ground. To change the configuration, the unit needs to be removed from the ground and reconfigured. Ensure the geophone sensors are placed in compacted soils and submerged at least 15 cm (0.5 ft.). The system was carefully hidden from the public eye and from animal disturbance to avoid tampering.

- Depending on power source option:

    - *12V battery Source*: Dig a hole large enough to fit the geophone unit and battery side by side and deep enough to cover the unit by 15 to 30 cm (0.5 to 1 ft.) of soil. Water seal the unit (caulk the cable glands outlets). Store the unit and the 12 battery in separate trash bags. Seal the trash bags, and cover the unit with compacted soil.

    - *Solar panel Power Source*: Dig a hole large enough to fit the geophone unit next to the solar panel control box. Water seal the unit (caulk the cable glands outlets). Store the unit and the 12 battery in separate trash bags. Seal the trash bags, and cover the unit with compacted soil.

- *Note:* It may be easier to store the unit in a trash bag prior to placing it into the hole. Make sure to compact the soil that covers the unit to ensure the hole does not flood. *Note:* For a more permanent setup, rather than burying the instrument in a hole, the instrument can be mounted securely to a pole.

1.4.2.4 Accessing Raspberry Pi system for data download

To access the Raspberry Pi system, connect your computer with the Pi system through the ethernet cable connection. Set the SSH client login to: pi@10.0.0.42 (or the name on the front of the Raspberry Pi system) and the password to: ***Geomote***.

Note: When accessing the Raspberry Pi system it is useful to ensure data collection is not interrupted, do not remove data until white LED on the Raspberry Pi system flashes three times.

To pull the data off the geophone system remotely, use the SSH File Transfer Protocol (SFTP) client on a laptop such as ***FileZilla*.** In the ***FileZilla*** app, set the site manager with the following specifications:

Protocol: SFTP –SSH File Transfer Protocol
Host: 10.0.0.42

Connect to the site and locate the data. The folder path is:
home/pi/GeoSeismic/GeomoteDue/Data.

Note: The data is organized by the date and time of day. The format of the data should be: *.int32*. The file is structured as a series of four 32-bit integers: Time, Channel 1 reading, Channel 2 reading, and Channel 3 reading.

1.4.3 Basic Analysis Procedure

Once the data has been exported in the .int32 format, use the geophone MATLAB script: *GeophoneReader,* which is included at the end of this appendix to construct subplots for each sensor. A step-by-step, detailed description is provided as comments within the script.

1.5 PART 2: PRELIMINARY ANALYSIS

1.5.1 Methods

Ground conditions were collected at 100Hz with a *GeoMoteShield* unit positioned on a cliff top located at Beverly Beach State park, 7 Miles north of Newport, Oregon. The positioning of the sensors is detailed in Figure 11 and Table 1. The relative distance from which the sensors are positioned from the road and cliff edge is detailed in Table 3. The geophone unit was stationed in this position for a total of three weeks between September 28, 2019 and November 8, 2019 at varying gain settings (4, 8 and 16 gain levels), as shown in Table 2. A 12V battery was connected to the sensor via the ECO Solar convertor and replaced weekly. The geophone sensors were installed 30 cm (1ft) underneath the ground into compact soil mixture of sand, gravel and soil. The geophone unit and 12V battery was stored and sealed in separate bags and covered with compacted soil to avoid tampering from the public and animal disturbance.

Table 1. Site positioning of the Geophone Unit. (Coordinate System: OCRS Salem NAD 1983 2011 TM).

Item	x-value (m)	y-value (m)
Geophone 1	27164.780	44611.165
Geophone 2	27152.553	44616.602
Geophone 3	27173.268	44640.806
Geophone Unit	27169.144	44625.211

Table 2. Testing date and Gain setting.

Test	Gain	Dates
1	4-bit	Sept. 28 - Oct. 04, 2019
2	8-bit	Oct. 13 - Oct. 18, 2019
3	16-bit	Nov. 03 - Nov. 08, 2019

Table 3. Reference of geophone positioning and surroundings.

Geophone	Distance from Road (m)	Distance from Bluff (m)
1	27	3
2	3	25
3	17	6

The local traffic noise was relatively high in this area and impacted the overall readings. Considerations were made when processing the data discussed in the Data Analysis section.

Wave buoy data [CDIP, http://cdip.ucsd.edu] provided an estimate for the significant wave heights the cliff was exposed to every 30mins. The wave buoy station was the UMPQUA OFFSHORE: OR–139, located at latitude: 43.77182 N and longitude: -124.54950 E at a depth of 186m, Figure 10. This buoy was selected because it is the closest buoy site with wave data obtained by CDIP to the testing site. It is located 70 miles SW of the tested cliff and roughly 17 miles off-shore, west of the city of Umpqua, OR. The data produced by geophone unit was compared to the buoy data to quantify the accuracy of the geophone system in evaluating wave height.

Figure 10. Location of CDIP buoy and Geophone test site near Beverly Beach.

Figure 11. Aerial view of test site. With the positioning of the geophone system. Reference Table 1 for specific positioning.

1.5.2 Data Analysis

The data was processed using the MATLAB Script, *GeophoneReader_downsmapling,* provided in this appendix. The geophone produced separate files for each day of testing. Since the files were calibrated each day, datasets that were obtained mid-day initially was excluded due to calibration differences in the data. The data was initially recentered about zero to make it easier to visualize the data. A moving average window (1, 5, 10, 15 and 30 mins.) was used to normalize the data and filter out the road noise produced by the nearby highway. More outliers were removed from the dataset that was greater than 100* Standard Deviation. The data was then down sampled to single points every 30mins, equaling a total of 48 points per 24 hours (1 day), the same intervals over which the CDIP wave data was reported. The graph produced four graphs: 1. Shifted dateset about zero, 2. Absolute value of shifted dataset about zero, 3. Average moving window applied to the dataset and 4. Amplitude of dataset.

The downsampled dataset was then compared to the significant wave heights data recorded by the Umpqua buoy. The geophone data were offset by +30 mins to account for the time change (RTC) between the two systems (+1 hr.) and travel time/distance of waves from the buoy to test site (-30 mins). The correlation coefficient (R^2 value) was used to determine if the amplitudes recorded by the geophone system could reliably predict the significant wave heights the cliff is exposed to. Generally, R^2-values of >0.50 are considered significant.

1.6 RESULTS/OBSERVATIONS

The ground motion data observed on the site at Beverly Beach varied drastically between the varying test dates (gain level settings: 4, 8 & 16). The ground motions observed during the 4 and 16 level gain settings was considered insignificant and the R^2-values ranged between $1.0x10^{-4}$ to 0.01, displaying no correlation between the cliff top ground motion and significant wave height the cliff was exposed to. Table 4 summarizes the R^2-values determined from the ground motion recorded at the three gain level settings.

The ground motions observed using a gain level of 8 was the only data collected that was considered significant. The readings between the three channels varied significantly. The ground motion data observed at the cliff edge through Channel 1 (3 m from cliff edge) revealed to have had the highest probability of predicting the cliff exposure wave heights with an R^2-value of 0.702 (moving average of 30-mins). Observations at Channel 2 (25 m from cliff edge) produced an insignificant R^2-value of 0.10 and Channel 3 (6m from cliff edge) had elevated R^2-value similar channel 1 but a lower degree, an insignificant R^2-value of 0.41. For Channel 2 and 3, the local ocean wave's noise appears to be insignificant and the signals are dominated by the local traffic noise, shown in Figures 13 and Figure 15. The data implies that proximity of Channel 2 and 3 to the bluff (Figure 11 and Table 3) caused the sensors to detect less wave action and more road noise. Since Channel 3 was closer to the cliff edge than channel 2, the signals were not as dominated by local traffic noises. This would account for why the sensors closer to the road followed a similar pattern one would expect for daily traffic levels, an increase of seismic movement during the day and at the am and pm rush hours as displayed in Figure 16.

A various moving average window was used to remove outside seismic waves produced by external sources. Using several moving average windows, it is notable that the R^2-value increased logarithmically as the moving average window increased. Figure 12 provides graphs displaying the R^2-values for all three channels with varying moving average windows. This emphasizes that there is a correlation between the determined R^2-values and the moving average window sizes used in analyzing the seismic data.

The geophone sensor is set to calibrate upon powering on the unit and then at midnight each day of operation. As a result, the calibrations were skewed on the first day of installation where the sensor was installed with significant traffic in the middle of the day. As a result, the impact of including these partial day datasets on the R^2 value was examined and shown in Table 4, 5 and 6. The R^2-value decreased when half days were considered by 0.02-0.05 on average (dependent on moving average window).

Between the three test dates, it is notable that the average significant wave heights the cliffs were exposed to varied (Table 4). The average wave heights during the gain level 8 test dates were on

average 1.4m greater than the other two test dates. The gain level 8 test dates standard deviation was at least 0.3m. greater than the other test dates. This likely accounts for why the other two test sets (4 and 16 gain levels) ground motion observations displayed no correlation between the significant wave heights data and the geophone channels. The waves during the gain level 4 test dates may have been large enough in magnitude to be detected but the gain setting of geophone unit was too lower to detect the local wave noises over the traffic noise. The sensitivity of the geophone unit during the gain level 16 test seemed to be set high enough to detect the local wave noises but the wave activity was too low to be detected by the system.

Table 4. Summary of Statics of CDIP Significant Wave Height Data.

Gain Level	Average (m)	Standard Deviation (m)	Median (m)
4	1.91	0.79	1.83
8	3.29	1.22	3.19
16	1.4	0.32	1.35

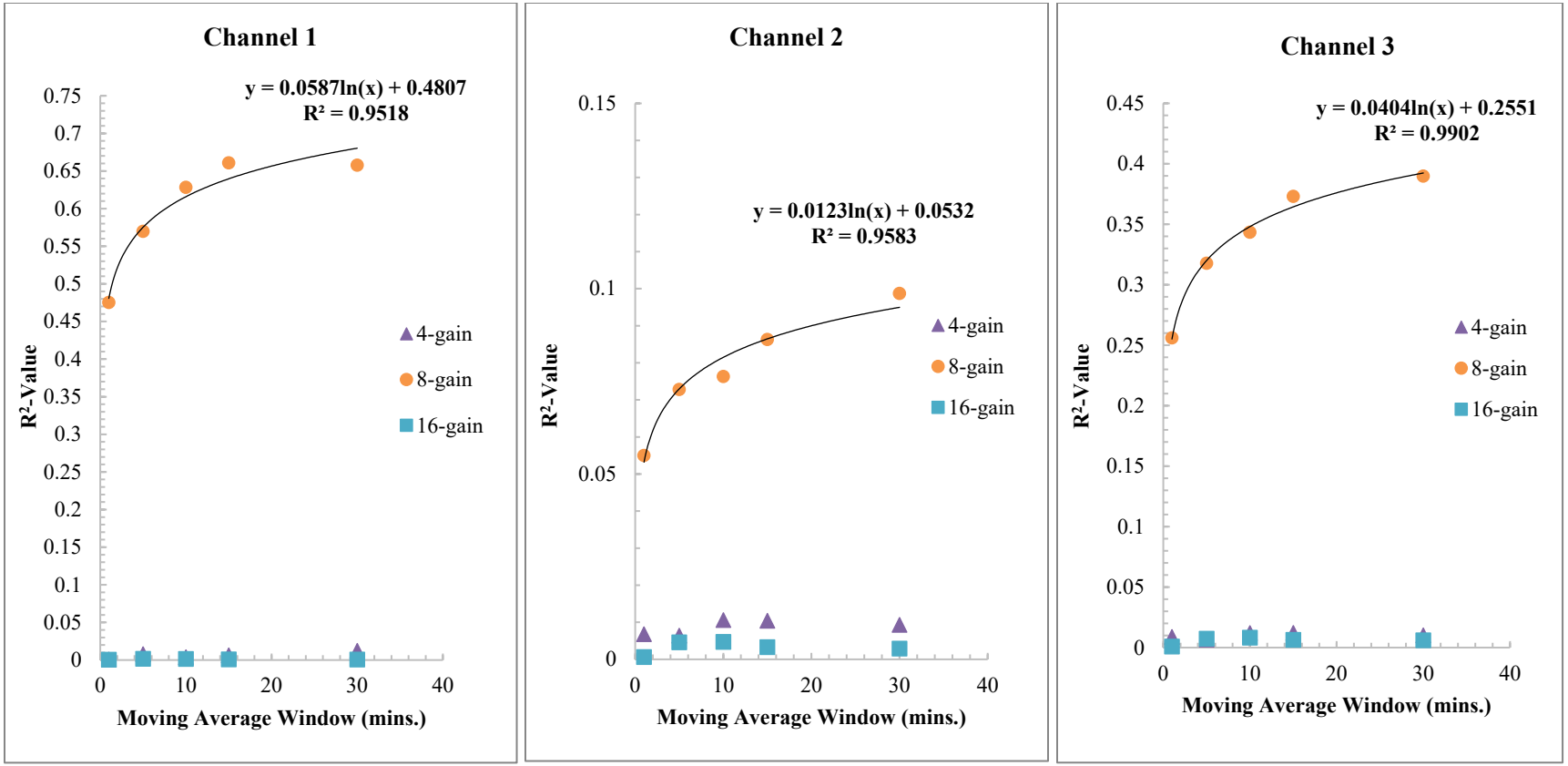

Figure 12. The down sampled data for all three channels and gain settings with varying moving averages used in analysis.

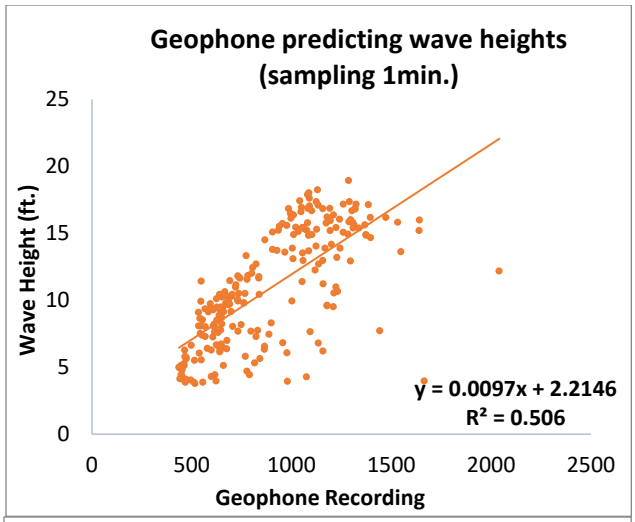

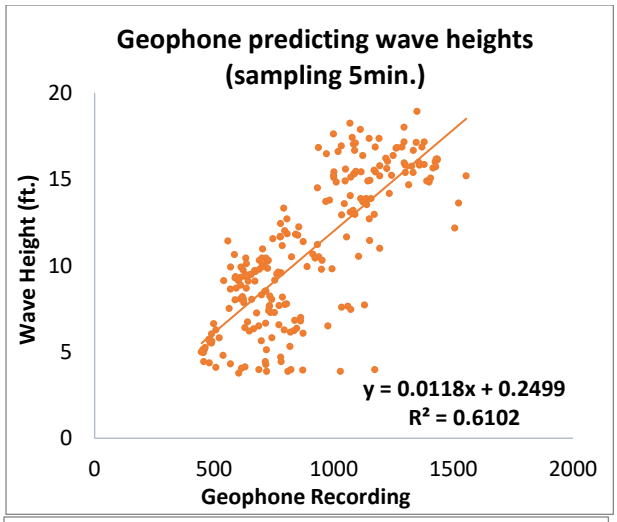

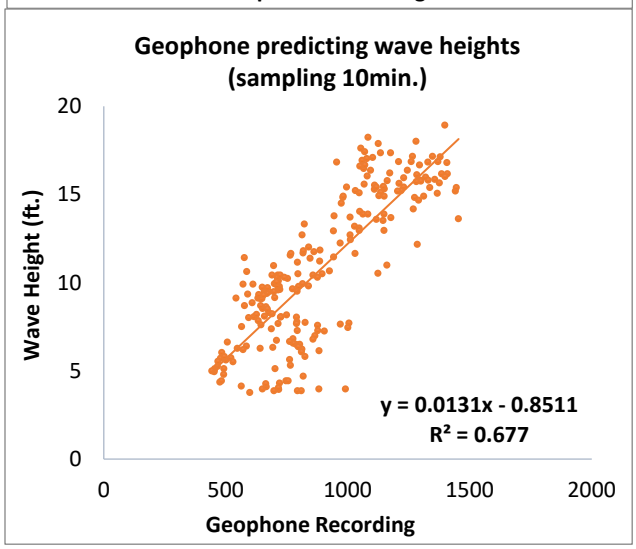

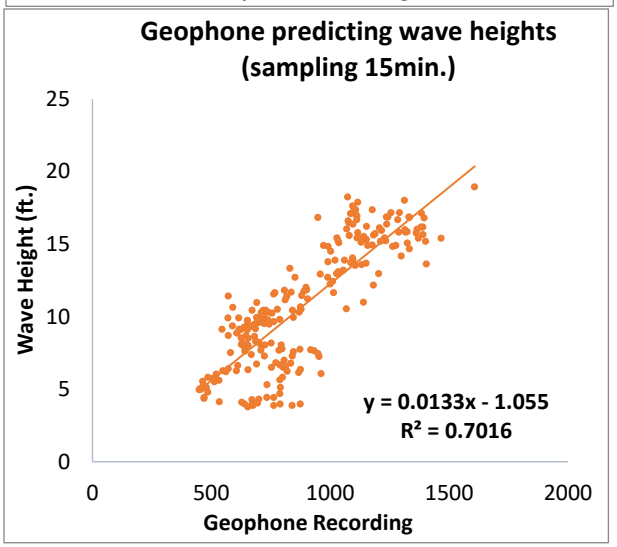

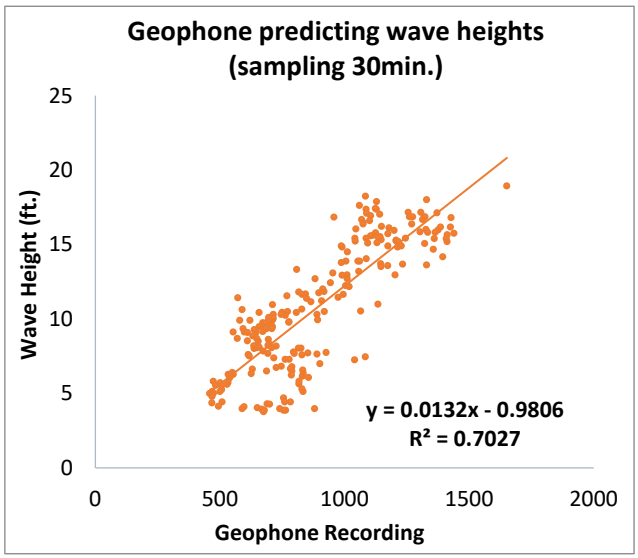

Figure 13. The downsampled data for Channel 1 (closest to cliff) data with gain setting of 8. Showing the seismic observations versus the Umpqua buoy significant wave height with varying moving averages in which the data was analyzed over (1, 5, 10, 15, 30 mins).

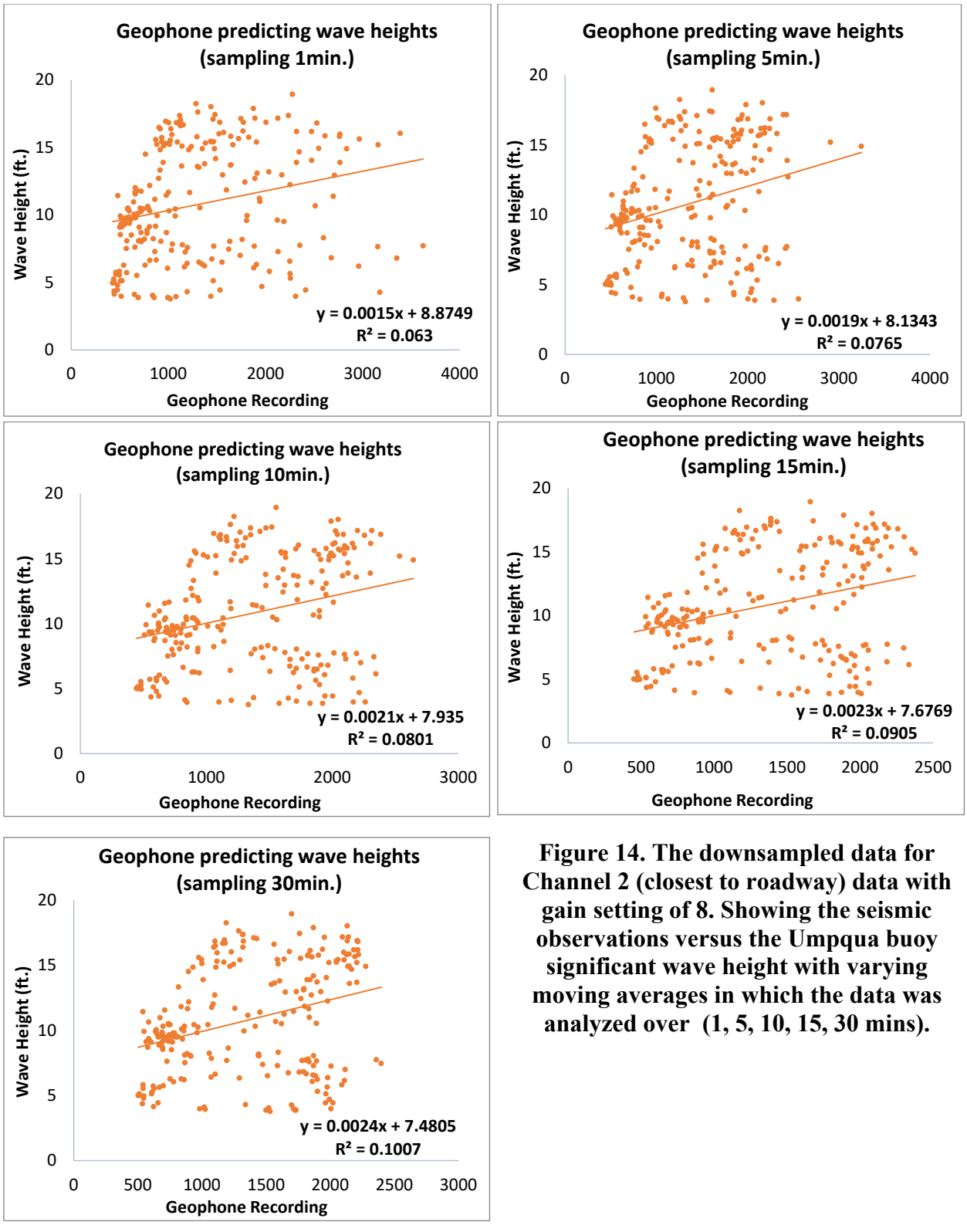

Figure 14. The downsampled data for Channel 2 (closest to roadway) data with gain setting of 8. Showing the seismic observations versus the Umpqua buoy significant wave height with varying moving averages in which the data was analyzed over (1, 5, 10, 15, 30 mins).

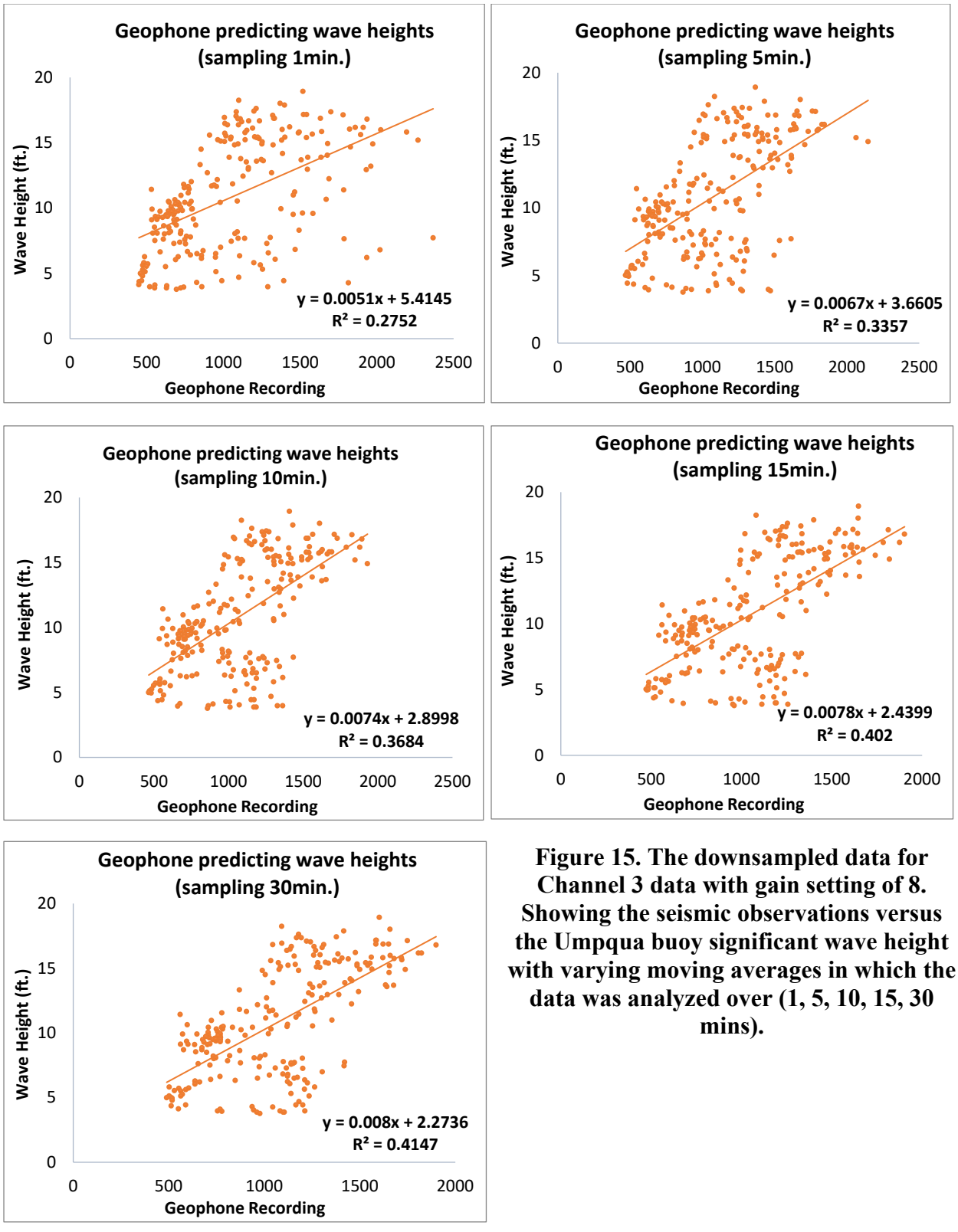

Figure 15. The downsampled data for Channel 3 data with gain setting of 8. Showing the seismic observations versus the Umpqua buoy significant wave height with varying moving averages in which the data was analyzed over (1, 5, 10, 15, 30 mins).

Table 5. Correlation coefficients (R2-values) of the Channels

Channel	Moving Average Window (min.)	R^2-values		
		4-gain	8-gain	16-gain
1	1	3.00E-03	**0.506**	3.40E-03
	5	8.00E-05	**0.610**	4.00E-05
	10	3.00E-04	**0.677**	5.00E-05
	15	2.00E-04	**0.702**	2.00E-04
	30	2.00E-04	**0.703**	2.00E-04
2	1	0.024	0.063	1.00E-05
	5	5.30E-03	0.077	1.70E-03
	10	0.029	0.077	1.30E-03
	15	0.030	0.091	4.00E-04
	30	0.028	0.101	2.00E-04
3	1	0.019	**0.275**	4.00E-05
	5	0.020	**0.336**	3.10E-03
	10	6.00E-03	**0.270**	3.00E-03
	15	9.10E-03	**0.402**	1.50E-03
	30	0.02	**0.415**	1.10E-03

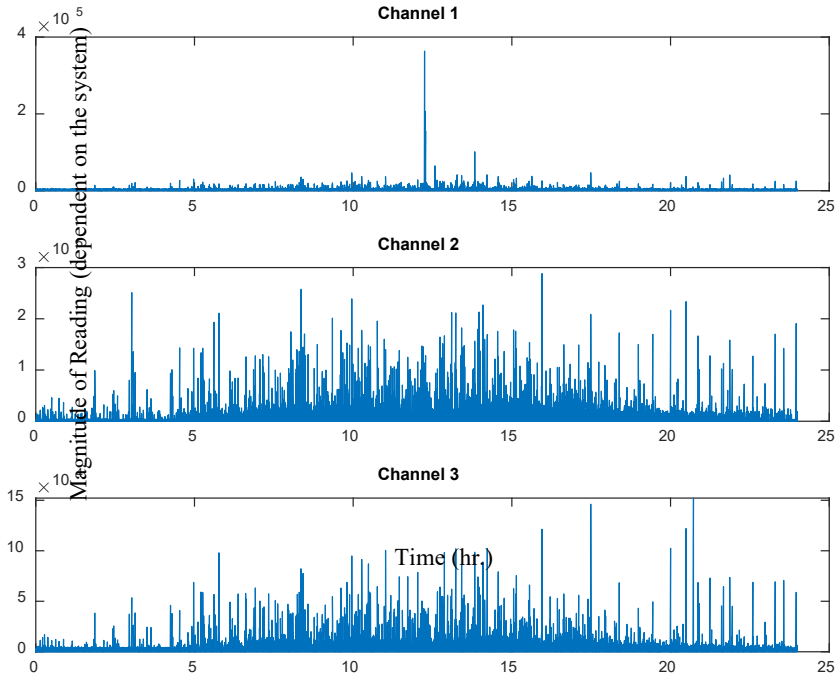

Figure 16. Example of raw data of ground motions recorded over a span of one day, displaying an increase in magnitude of motion in Channels 2 and 3. (Test date: Oct. 14, 2019).

1.6.1 Graph (Matlab Script)

There were four tables produced by the Matlab script: 1. Shifted Raw dateset about zero, 2. Absolute value of shifted Raw dataset about zero, 3. Average moving window applied to the dataset and 4. Amplitude of dataset.

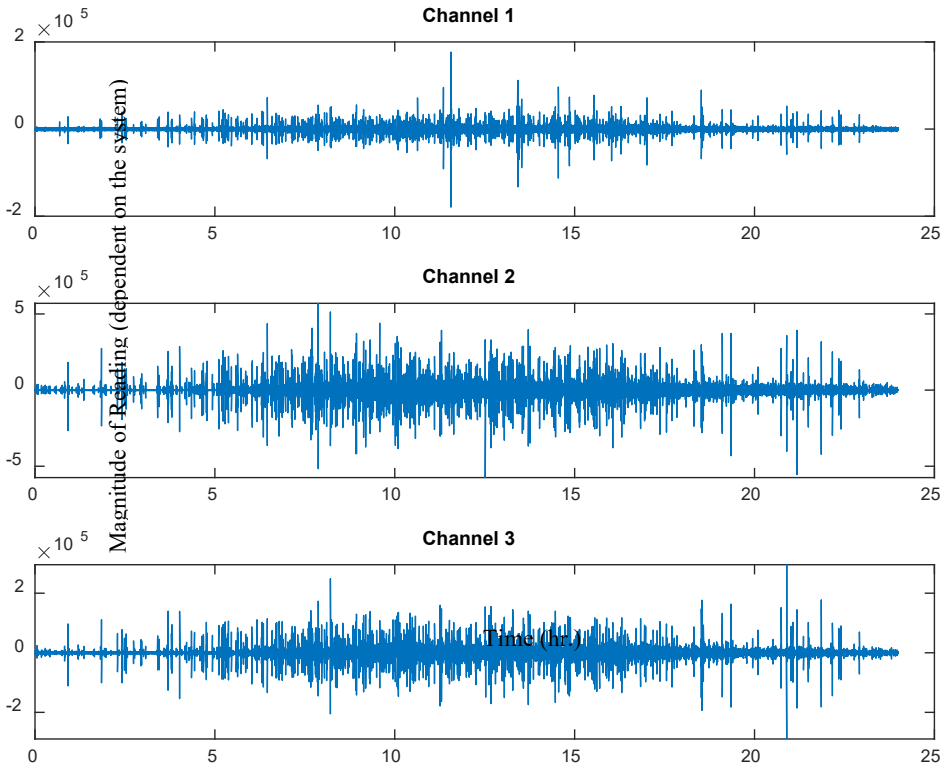

Figure 17. Shifted raw geophone data around zero (Test date: Nov. 7, 2019).

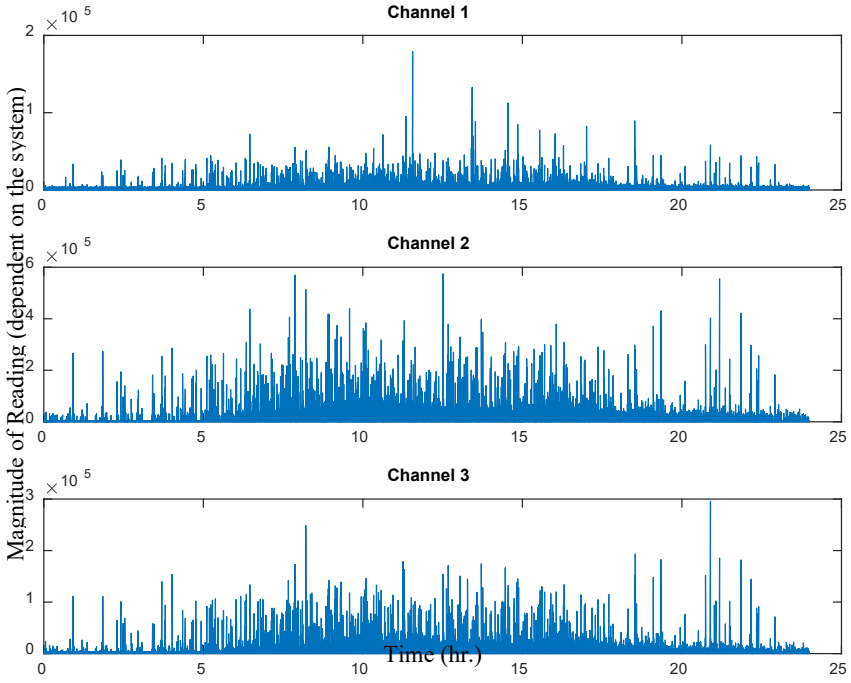

Figure 18. Absolute shifted raw geophone data around zero (Test date: Nov. 7, 2019).

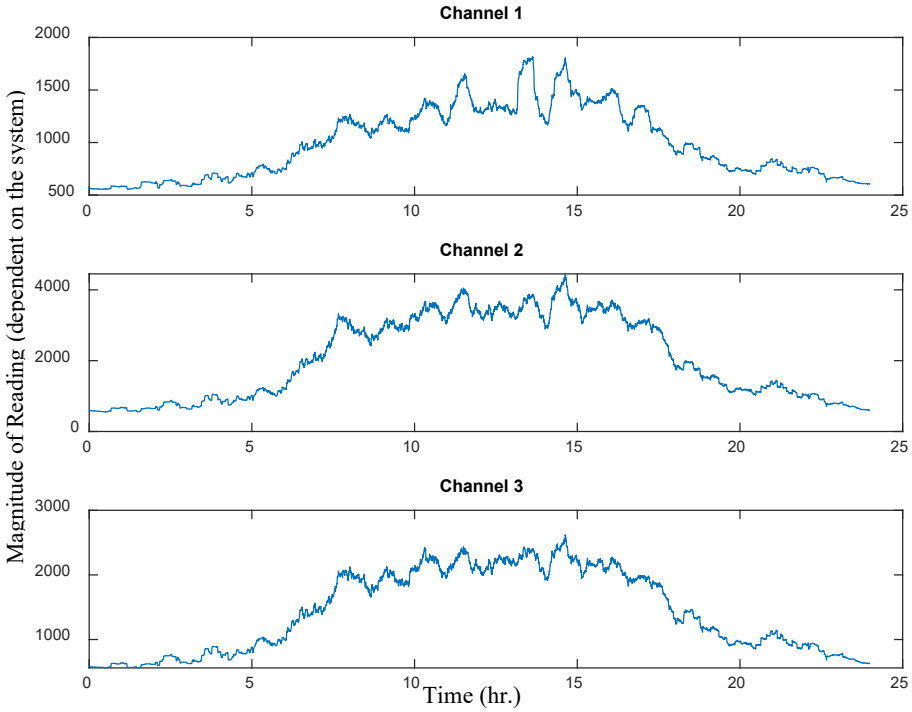

Figure 19. Normalized data using a moving average window of 30mins. (Test date: Nov. 7, 2019).

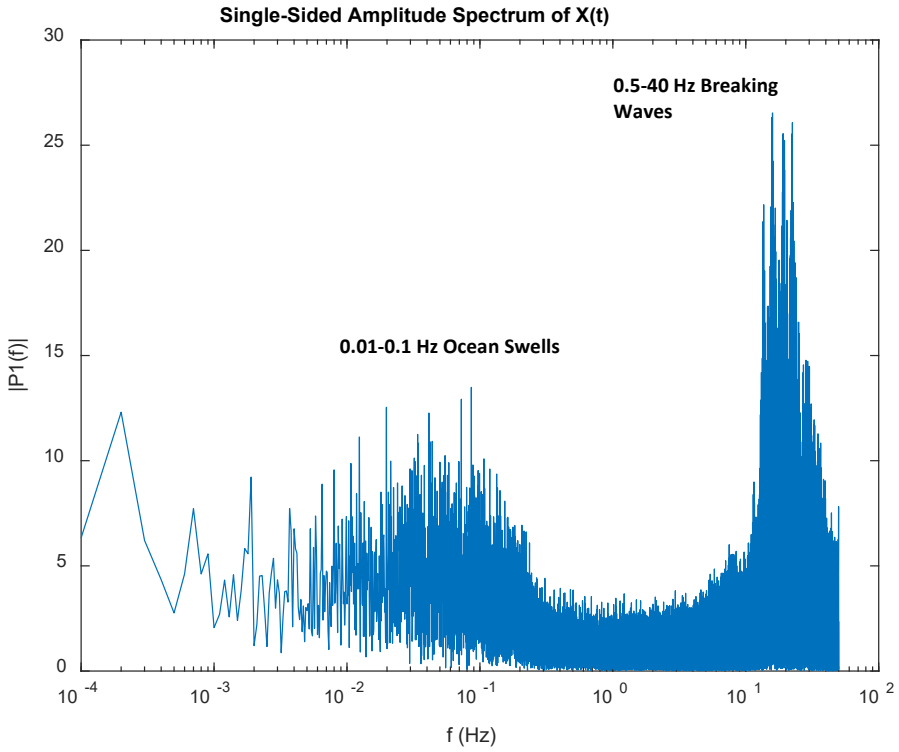

Figure 20. Amplitude values displaying the frequencies recorded by geophone (Ranging from 0.01 to 45 Hz.) (Test date: Nov. 7, 2019).

1.7 DISCUSSION

This short-term observation of the GeoMoteShield geophone system in monitoring coastal ground motions is consistent with previous studies [*Adams et al.*, 2002, 2005; *Pentney*, 2010; *Lim et al,.*2011; *Young et al.*, 2011, 2012, 2013]. The degree of ground motion detected is dependent on a variety of parameters. The ocean generated cliff motion decayed inland is consistent with previous studies [Adams et al., 2005; Pentney, 2005]. *Adams et al.,* [2005] suggested that cliff motion decay inland and might cause cliff weakening through stain-related fatigue processes. There is a correlation between the determined R^2-value and the sensors proximity to the cliff top edge, shown in Figure 21. For the 8-gain test, there is an exponential relationship between the R^2-value and distance of sensors from clifftop edge. There is also a correction between the R^2-value and the sensors proximity to Highway 101 for the gain level 8 test, shown in Figure 22. The R^2-value increases as the geophone sensor is further away from the road which generates excessive external noise.

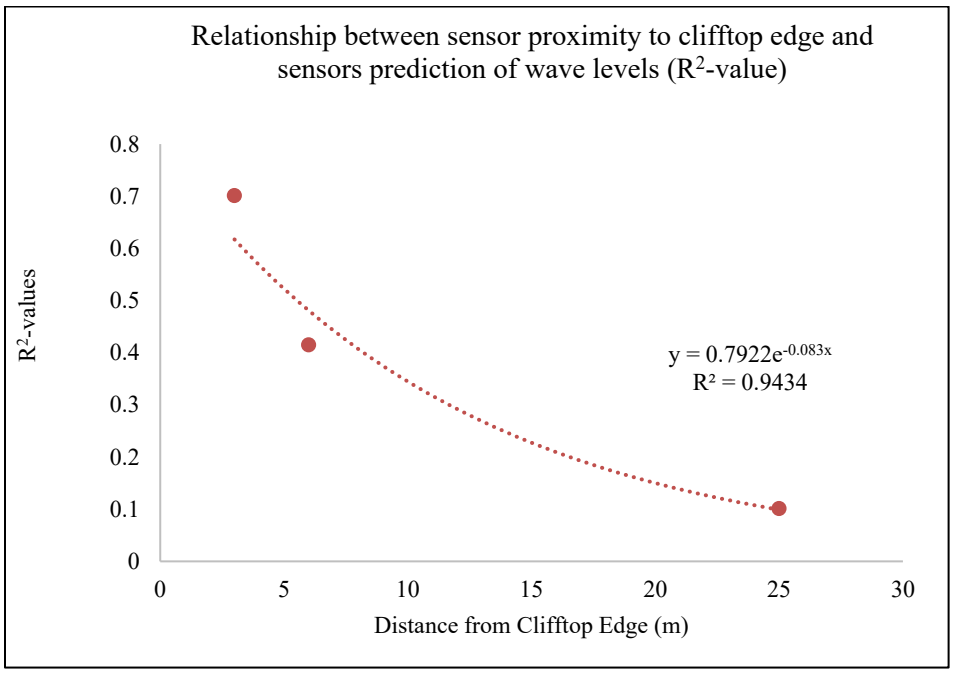

Figure 21. Exponential relationship of sensor proximity to clifftop edge and sensors prediction of wave levels (R^2-value).

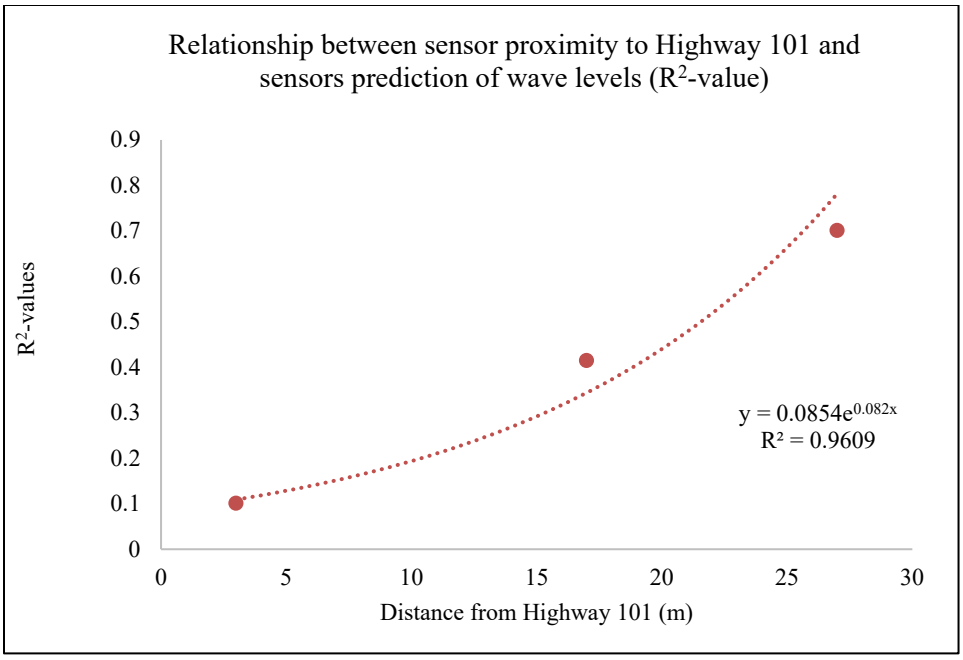

Figure 22. Exponential relationship of sensor proximity to Highway 101 and sensors prediction of wave levels (R^2-value)

The ground motion observed at the clifftop is similar to what *Young et al.* [2011] discovered on California clifftop sites. The magnitude of wave energy detected by the sensor on the cliff-top edge increased as tidal levels and incident levels increased. Based on the observations when the tidal and significant wave height levels were greater, there was a stronger correlation of the sensors predicting the wave levels (8-gain test).

Graph four (Figure 20) shows that the geophone recorded frequencies values range between 0.01 to 45 Hz which is similar to *Young et al.* [2011, 2013] and *Earlie et al.* [2015] determined. *Young et al.* [2011, 2013] stated that frequencies waves that range from 0.01 to 0.1Hz are produced by ocean swells and frequencies waves that range from 0.5 to 40Hz are produced by breaking ocean waves. The geophone recordings corroborate what *Young et al.* and *Earlie et al*. found.

1.7.1 Suggestions for Future Research

This new and inexpensive geophone system shows real promise in being used in monitoring wave activity. This study was meant to be a preliminary study to provide a proof of concept of utilizing the geomote sensors for this application. Since the study is limited due to the relatively short monitoring period of recording ground motion data as well as limited evaluation of the other parameters that effect coastal erosion. However, based on these results and previous studies [*Adams et al.*, 2002, 2005; *Pentney*, 2010; *Lim et al.,* 2011; *Young et al.*, 2011, 2012, 2013], the system has the potential to be used in monitoring the variation of wave heights but it would require evaluating more parameters that effect the ground motion recordings: distance from the bluff, the magnitude of wave energy, morphology etc. In order to deploy these systems more

rigorously for monitoring coastal processes, additional tests are recommended. Suggestions are provided below in the respective sections.

1.7.1.1 Alterations to Arduino Code

The current Arduino is set to calibrate the data every day which made it more difficult to compare dataset from different days. If the system is set to calibrate every time it is setup, datasets consisting of consecutive days could be evaluated easier. Tidal patterns and wave energy variations will be easier to distinguish with larger datasets.

1.7.1.2 Location Sensor

A large portion of ODOT coastal infrastructure is located near coastal cliffs or bluffs which creates the issue of ground motion interference from local traffic. An overall evaluation of the sites would need to be conducted to determine the optimal location to position the sensors. Its proximity to the road and the cliff edge is crucial in detecting the wave action only and minimizing noise from traffic. *Young et. Al.* [2011] positioned the seismometers at varying locations from the cliff edge and determined that ground motion decayed rapidly with inland distance from the cliff. Similar methods could be used with test and evaluating this sensor.

1.7.1.3 Evaluations of Gain Setting

Based on the current observations, an optimal gain setting has not been determined. Observations show that the gain settings is dependent on magnitude of wave energy and proximity to the clifftop. An optimal level will need to be determined that can detect a wide range of wave sizes and proximity to the other noises besides local ocean waves. The gain setting may be dependent on time of year, during the winter months wave energy is greater than during the summer months.

1.7.1.4 Regular Scans/Video Monitoring: Existing morphology

The morphology of a cliff face also interferes with how ground motions transfers through the mediums. *Lim and Rosser et. al.* [2011] observed that the morphology has a significant influence on wave energy flux and impact timing at the cliff face. The slope of the cliff face, as well as the beach morphology could impact the ground motion detection. Although no video/scan monitoring was used in this preliminary test, monitoring of the cliff face may be useful in quantifying the cliff change and existing morphology. *Earlie et. al,.* [2015] used a GoPro® waterproof video camera that was GPS time synced. The video camera provided a qualitative but detailed account of the hydrodynamics the cliff face endured. *Lim and Rosser et. al*. [2011] used a lidar survey of the coastal corridor to quantify an understanding of the foreshore morphology. Similar methods could be employed for testing this geophone unit. A terrestrial lidar survey of the cliff can be conducted regularly (weekly) and a camera can be positioned facing the cliff face to monitor the wave energy to quantify the change of the cliff face and ground motion noises. Another camera could be positioned facing the road so it can record the local traffic noises, therefore be used in canceling out the residual noises in the data.

An analysis of the soil structure may be useful as well to determine how wave frequencies travel through the cliff medium.

1.8 CONCLUSION

Ground motions on a cliff top was observed using a *GeoMoteSheild* system to investigate the potential the unit has in recording ground motions by local ocean waves. Results from this primary test indicates that the system has a high potential of being used in coastal monitoring. Of the trials, the 8 gain level test was the only test that showed that the sensor was able to predict cliff wave exposure levels. It indicated that there is a correlation between the sensors proximity to clifftop edge and the sensors prediction of wave levels (R^2-value). When the sensor is positioned closer to the cliffs edge, it is able to better detect local wave action. The magnitude of wave levels also plays a role in determining the most optimal gain setting to monitor wave action. It was concluded that the wave levels, gain levels and proximity to the clifftop all play a significant role the unit's ability to detect wave energy.

1.9 REFERENCES

Adams, P. N., R. S. Anderson, and J. Revenaugh (2002), Microseismic measurement of wave-energy delivery to a rocky coast,Geology,30(10),895–898.

Adams, P. N., C. D. Storlazzi, and R. S. Anderson (2005), Nearshore wave-induced cyclical flexing of sea cliffs,J. Geophys. Res.,110, F02002,doi:10.1029/2004JF000217.

Allan, J.C., and Komar, P.D., 2002, Extreme storms on the Pacific Northwest coast during the 1997–98 El Niño and 1998–99 La Niña: Journal of Coastal Research, v. 18, no. 1, p. 175–193

Bossolasco, M., G. Cicconi, and C. Eva (1973), On microseisms recorded near a coast, Pure Appl. Geophys.,103(1), 332–346, doi:10.1007/BF00876409.

British Geological Survey (BGS), 2020, "Seismic Waves." Seismic Waves | Earthquakes | Discovering Geology | British Geological Survey (BGS), UK Natural Environment Research Council, Jan. 2020, www.bgs.ac.uk/discoveringGeology/hazards/earthquakes/seismicWaves.html.

Dickson, M. E., and R. Pentney (2012), Micro-seismic measurements ofcliff motion under wave impact and implications for the development ofnear-horizontal shore platforms, Geomorphology,151, 27–38.

Dickson, M. E., H. Ogawa, P. S. Kench, and A. Hutchinson (2013), Sea-cliff retreat and shore platform widening: Steady-state equilibrium?,Earth Surf. Processes Landforms, 38(9), 1046–1048.

Earlie, C. S., Young, A. P., Masselink, G., & Russell, P. E. (2015). Coastal cliff ground motions and response to extreme storm waves. Geophysical Research Letters, 42(3), 847-854.

Hormann, Liz. "ODOT's Climate Change Adaptation Strategy Report." Www.oregon.gov, Apr. 2012, www.oregon.gov/ODOT/Programs/TDD%20Documents/Climate-Change-Adaptation-Strategy.pdf.

Mills, A. K., Bolte, J. P., Ruggiero, P., Serafin, K. A., Lipiec, E., Corcoran, P., & Lach, D. (2018). Exploring the impacts of climate and policy changes on coastal community

resilience: simulating alternative future scenarios. Environmental modelling & software, 109, 80-92.

Pentney, R. (2010). Seismic Measurements of Wave Energy Delivery to a Rocky Coastine: Okakari Point, Auckland, New Zealand (Doctoral dissertation, University of Auckland).

Lim, M., N. J. Rosser, D. N. Petley, and M. Keen (2011), Quantifying the controls and influence of tide and wave impacts on coastal rock cliff erosion, J. Coastal Res., 27(1), 46– 56.

Senfaute, G., Duperret, A., & Lawrence, J. A. (2009). Micro-seismic precursory cracks prior to rock-fall on coastal chalk cliffs: a case study at Mesnil-Val, Normandie, NW France. Natural Hazards & Earth System Sciences, 9(5).

Ruggiero, P., Kratzmann, M. G., Himmelstoss, E. A., Reid, D., Allan, J., & Kaminsky, G. (2013). National assessment of shoreline change: historical shoreline change along the Pacific Northwest coast. US Geological Survey.

Rubin, Marc J. "Efficient and automatic wireless geohazard monitoring." PhD diss., Colorado School of Mines. Arthur Lakes Library, 2014.

Young, A. P., P. N. Adams, W. C. O'Reilly, R. E. Flick, and R. T. Guza(2011), Coastal cliff ground motions from local ocean swell and infra-gravity waves in southern California,J. Geophys. Res.,116, C09007,doi:10.1029/2011JC007175.

Young, A. P., R. T. Guza, P. N. Adams, W. C. O'Reilly, and R. E. Flick(2012), Cross-shore decay of cliff top ground motions driven by localocean swell and infragravity waves,J. Geophys. Res.,117, C06029, doi:10.1029/2012JC007908.

Young, A. P., Guza, R. T., Dickson, M. E., O'Reilly, W. C., & Flick, R. E. (2013). Ground motions on rocky, cliffed, and sandy shorelines generated by ocean waves. Journal of Geophysical Research: Oceans, 118(12), 6590-6602.

1.10 SUPPLEMENTAL DATA

Table 6. R2-value of Geophones at predicting the significant wave heights the cliff was exposed (4-gain level setting).

Channel	Moving Average	All	No-13	No-18	Whole-Day
1	1	0.0006	0.0007	0.0005	0.0055
1	5	0.0079	0.00008	0.0052	0.0015
1	10	0.0037	0.0009	0.0015	0.0084
1	15	0.0062	0.0009	0.0028	0.0076
1	30	0.0122	0.0003	0.0070	0.0025
2	1	0.0068	0.0262	0.0085	0.0394
2	5	0.0064	0.0053	0.0134	0.0499
2	10	0.0106	0.0350	0.0200	0.0590
2	15	0.0104	0.0333	0.0205	0.0693
2	30	0.0093	0.0907	0.0189	0.0540
3	1	0.0088	0.0219	0.011	0.0355
3	5	0.0066	0.0204	0.0147	0.0438
3	10	0.0121	0.0323	0.0134	0.0626
3	15	0.0122	0.0302	0.0243	0.0694
3	30	0.0101	0.0266	0.0213	0.0546

Table 7. R2-value of Geophones at predicting the significant wave heights the cliff was exposed (8-gain level setting)

Channel	Moving Average	All	No-13	No-18	Whole-Day
1	1	0.4753	0.4984	0.4275	0.4621
1	5	0.5697	0.6074	0.4942	0.5468
1	10	0.6282	0.6689	0.5574	0.6150
1	15	0.6608	0.6942	0.5835	0.6441
1	30	0.6577	0.7016	0.5944	0.6559
2	1	0.0550	0.0581	0.0627	0.0676
2	5	0.0728	0.0776	0.0504	0.0561
2	10	0.0763	0.0776	0.4990	0.0556
2	15	0.0863	0.0922	0.058	0.0647
2	30	0.0987	0.1054	0.0685	0.0766
3	1	0.2561	0.2702	0.2393	0.2626
3	5	0.3177	0.3410	0.2536	0.288
3	10	0.3434	0.3692	0.2734	0.3111
3	15	0.3730	0.4013	0.3031	0.3437
3	30	0.3898	0.4199	0.3212	0.3650

Table 8. R2-value of Geophones at predicting the significant wave heights the cliff was exposed (16-gain level setting)

Channel	Moving Average	All	No-13	No-18	Whole-Day
1	1	0.0005	0.0021	0.0012	0.0081
1	5	0.0017	0.00004	0.00033	0.0003
1	10	0.0015	0.00003	0.0043	0.0010
1	15	0.0008	0.00001	0.0062	0.0016
1	30	0.0006	0.00002	0.0057	0.0021
2	1	0.0006	0.00008	0.0026	0.0005
2	5	0.0046	0.0025	0.0083	0.0036
2	10	0.0047	0.0021	0.0108	0.0048
2	15	0.0033	0.0011	0.0114	0.0051
2	30	0.0029	0.0009	0.0117	0.0054
3	1	0.0008	0.00005	0.0020	0.000005
3	5	0.0074	0.0040	0.0910	0.0027
3	10	0.0082	0.0042	0.0123	0.0041
3	15	0.0064	0.0627	0.0133	0.0047
3	30	0.006	0.0026	0.0131	0.005

1.11 SCRIPTS

Basic *GeophoneReader* Script
Description:
The output of this script 3 basic graphs one for each geophone showing the raw data recorded by the geophone. The data is shifted to range between 0 to 1. Inputs into this script are the FILENAME for both the *gfile* and *fs* parameter, which determines what dataset is being analyzed.

Script:

```
%File number
gfile = fopen("FILENAME.int32");
%Direct to the file folder
fs = dir(FILENAME.int32');
%Subdividng the dataset into correct format
n = fs.bytes/4/4;
%Interprets values in the file according to the form and size described by
%precision. Matrix size of 4 rows, n columns
data = fread(gfile,[4 n],"int");
%Closes the file after data removed
fclose(gfile);
%Transposes the data to 4 columns and n rows
datat = transpose(data);
%Determines the min. and max. of each channel
mins = min(data,[],2);
maxs = max(data,[],2);
%Determines the spread of the data set
ranges = maxs-mins;
%Data is normalized by removing the min. values from dataset
datanorm = data -mins;
%Normalize the data again by dividing normalized over the range of the
dataset
datanormz = datanorm./ranges (:,1);

%Plot each channel of the geophone in separate graphs
subplot (311);
plot(data(1,:),datanormz(2,:));
title('Channel 1')
subplot (312);
plot(data(1,:),datanormz(3,:));
title('Channel 2')
subplot (313);
plot(data(1,:),datanormz(4,:));
title('Channel 3')
```

***GeophoneReader_downsampling* Script**

Description:

The output of this script is 4 graphs: 1. Shifted dateset about zero, 2. Absolute value of shifted dataset about zero, 3. Average moving window applied to the dataset and 4. Amplitude of dataset.

Inputs into this script are the FILENAME for both the *gfile* and *fs* parameter, which determines what dataset is being analyzed. Another input in this script is *avewindowminutes* which alters the average moving window in which the data is analyzed over. The parameter *outliermultiplier* is another input in this script, it determines the degree at which outliers are removed based on how many standard deviations values it is from the average.

Script:

```
%variables to adjust
avewindowminutes = 30; %adjust me , try 1,5, 10, 15, 30
%Determines the moving average used that the data is analyzed over
moveavewindow= 100*60*avewindowminutes;
%Value used to limit the range of the data (used cancel excessive random loud
%noises)
outliermultiplier = 100;

%other variables
dswindow= 100*60*30;  %DONT" CHANGE!!! downsamples to measurements every 30
minutes;
% Open file in int.32 format
gfile = fopen("2019_11_05__00_00_01.int32");
%Directs to the specific file%
fs = dir('2019_11_05__00_00_01.int32');
%Organize the data in a 4 by n matrix
n = fs.bytes/4/4;
%Read specific file with a 4 by n matrix with a precision of integer
data = fread(gfile,[4 n],"int");
%Closed the opened gfile
fclose(gfile);
%Transposes the data from a from Rows to Columns
datat = transpose(data);
%Defining min. limits from the data matrix, column vector containing min.
value for each channel
mins = min(data,[],2);
%Defining max. limits from the data matrix, column vector containing max.
value for each channel
maxs = max(data,[],2);
%Compute the median values for each row (help cancel out some loud noises)
medians= median(data,2);
%Compute the standard deviation for each row
stdevs = std(data,0,2);
%Setting the range of the channel, Max-Min of each channel
ranges = maxs-mins;
%Shift data by removing the median from the datasets (Used to help
%cancel out excessive random loud noises)
```

```
datanorm = data - medians;

%For all values, if they are greater or less than 100*standard deviation of
the dataset, set value to 0 (removed it).
%If data is between 100*standard deviation of the datasets, keep the value
for i=2:4
    for j = 1:n
        if (datanorm(i,j) > outliermultiplier*stdevs(i))
            datanorm(i,j) =0;
        elseif (datanorm(i,j) < - outliermultiplier*stdevs(i))
            datanorm(i,j) =0;
        end

    end
end

%Rename the normalized data to datanormz
datanormz = datanorm;
%For all the datasets, divide the data
data(1,:) = data(1,:)/60/60/100;
%Figure 1 with graph detail for each Channel
figure;
 subplot (311);
 plot(data(1,:),datanormz(2,:));
 title('Channel 1')
 subplot (312);
 plot(data(1,:),datanormz(3,:));
 title('Channel 2')
 subplot (313);
 plot(data(1,:),datanormz(4,:));
 title('Channel 3')

%Determine the absolute values of the dataset
 datanormabs = abs(datanorm);
 %Figure 2 with graph detail displaying the absolute values
 figure;
 subplot (311);
 plot(data(1,:),datanormabs(2,:));
 title('Channel 1')
 subplot (312);
 plot(data(1,:),datanormabs(3,:));
 title('Channel 2')
 subplot (313);
 plot(data(1,:),datanormabs(4,:));
 title('Channel 3')
%For all values, determine the moving average of the datasets with varying
window values
%Then down sample the data after a moving average was determined with a
varying window value
for (i = 2:4)
    datanormmean(i,:) = movmean(datanormabs(i,:),moveavewindow);
    datanormmeands(i,:) = downsample(datanormmean(i,:), dswindow);
end
```

```
%Figure 3 with graph detail, plotting channel of the geophone in separate
%graphs (not downsampling the data)
figure;
 subplot (311);
 plot(data(1,:),datanormmean(2,:));
 title('Channel 1')
 subplot (312);
 plot(data(1,:),datanormmean(3,:));
 title('Channel 2')
 subplot (313);
 plot(data(1,:),datanormmean(4,:));
 title('Channel 3')

%Set data to be named junk for all values from 1 to 1000000
 junk = (data(3,1:1000000));
%Computes the discrete Fourier transform values for the dataset (used for
%signals buried in noise data)
Y = fft(junk);
%Sampling frequency
Fs =100;
%Length of signal values
L = 1000000;

%Compute the two-sided spectrum P2. Then compute the single-sided spectrum
%P1 based on P2 and the even-valued signal length L.
P2 = abs(Y/L);
P1 = P2(1:L/2+1);
P1(2:end-1) = 2*P1(2:end-1);

%Define the frequency domain f and plot the single-sided amplitude spectrum
P1.
%The amplitudes are not exactly at 0.7 and 1, as expected, because of the
added noise.
%On average, longer signals produce better frequency approximations.
f = (Fs*(0:(L/2))/L);
%Figure 4
figure;
semilogx(f,P1)
title('Single-Sided Amplitude Spectrum of X(t)')
xlabel('f (Hz)')
ylabel('|P1(f)|')
```